ISSN 1029-9599, Physical Mesomechanics, 2018, Vol. 21, No. 2, pp. 124–134. © Pleiades Publishing, Ltd., 2018.
Original Text © M. Acanfora, P. Gallo, N. Razavi, M.R. Ayatollahi, F. Berto, 2018, published in Fizicheskaya Mezomekhanika, 2018, Vol. 21, No. 1, pp. 30–40.

Numerical Evaluation of *T*-stress under Mixed Mode Loading Through the Use of Coarse Meshes

M. Acanfora[1], P. Gallo[1], N. Razavi[2]*, M. R. Ayatollahi[3], and F. Berto[2]

[1] *Department of Mechanical Engineering, Marine Technology, Aalto University, Espoo, 02150 Finland*
[2] *Department of Mechanical and Industrial Engineering, Norwegian University of Science and Technology, Trondheim, 7491 Norway*
[3] *Department of Mechanical Engineering, Iran University of Science and Technology, Tehran, 16846-13114 Iran*
* *e-mail: nima.razavi@ntnu.no*

Received March 09, 2017

Abstract—The present paper investigates the employment of coarse meshes in evaluating the *T*-stress with the displacement method. Several finite element analyses have been carried out with different mesh refinements and accuracies. Mode I and mixed mode I/II loadings have been considered in finite element analyses. Under mode I loading, single and double edge notched geometries have been considered, while plate with central crack has been considerd for mixed mode loading condition. The analyses are compared with the results by the well-nown stress based approach, and showed that the displacement method permits the evaluation of the *T*-stress with the employment of coarse meshes. By the way, several precautions must be taken when dealing with coarse and very coarse meshes.

DOI: 10.1134/S1029959918020054

Keywords: *T*-stress, displacement method, coarse mesh, mixed mode loading

1. INTRODUCTION

Failure of cracked components is governed by the stresses in the vicinity of the crack tip. Under small scale-yielding condition, a single parameter is used to characterize the crack-tip stress and as a fracture criterion. McClintock [1] clearly showed that a single parameter might not suffice to characterize the near-crack tip states under large scale yielding condition, when the stress triaxiality level is low. Example is given when considering nonhardening material under fully plastic condition, since the near-tip fields depend on the configuration. In such cases, several researchers have tried to develop new approaches, with the introduction of a second parameter to characterize the crack-tip condition [2–6]. The importance of the two-parameter approaches in linear elastic fracture mechanics analysis is increasingly being recognized for fracture assessments in engineering applications. One of such theories is the *T*-stress approach, in which the elastic *T*-stress [7] is taken into account in the description of the near-tip field. Analytical and experimental studies have shown that *T*-stress can be used as a measure of constraint for contained yielding, see for example [8, 9]. Despite its significance, few methods are available for calculating *T*-stress in case of mixed mode loading. Those methods that do exist are either restricted to simple geometries or need complex numerical analysis. An extensive review of analytical methods used for evaluating the *T*-stress is reported by Sherry et al. [10], while the integral equation method for multiple cracks with *T*-stress has been addressed by Chen [11].

Larsson and Carlsson [12] computed *T*-stress as the average difference between the σ_x for a specimen and the corresponding value obtained from the boundary layer approach where σ_x was obtained from the elastic-plastic finite element method. This analysis was carried out for mode I only.

Leevers and Radon [13] used a variational technique based on the theorem of minimum potential energy to estimate the *T*-stress for mode I. A similar approach was previously applied by [14] for mixed mode I and II. Knesl [15] also attempted to determine the *T*-

stress, according to the same technique in mode I. He used special types of element called crack-tip hybrid elements developed through a Hellinger–Reissner principle.

Using the properties of path independent integrals, Cardew et al. [16] and later Kfouri [17] suggested a method to obtain the *T*-stress under mode I loading. The method is based on an unpublished theorem proposed by Eshelby. Fett [18] proposed a closed form approximation for *T* for a mode I rectangular cracked specimen under tension and bending. Maleski et al. [19] has determined a modified stress difference method to calculate the *T*-stress, with extrapolation method, for mode I.

Limited number of contributions regard with the mixed mode. Path independent integrals were employed by Olsen [20] and Sladek et al. [21], to compute the *T*-stress for mixed mode loading using the boundary element technique. Seed and Nowell [22], to determine *T* for mixed modes I and II, represented a crack as a continuous distribution of edge dislocations. Distributed dislocation method were employed to derive the singular equations, which were solved numerically to find stress intensity factors.

The development of a unified finite element technique for calculating *T*-stress is envisaged. An interesting contribution to the topic has been provided by Ayatollahi et al. [23] that presented a technique for evaluating *T*-stress for mode I and II, involving finite element analyses. Moreover, methods for the calculation of the *T*-stress for any mixed mode I/II loading were proposed, without the need to evaluate the stress intensity factors.

In this paper the method presented in [23] is briefly recalled and applied by assuming different mesh refinements. This study aims to disclose novel outcomes concerning the reliability of the results by using coarse to fine meshes for mode I and for mixed mode loading.

2. FUNDAMENTAL CONCEPTS OF *T*-STRESS

Westergaard [24] studied the biaxial stress field for internal cracks in pressurized cylinders. The outcomes of the research demonstrated that it was possible to state the stresses and the shearing stress in the *x* and *y* directions as follows:

$$\begin{Bmatrix} \sigma_{xx} \\ \sigma_{yy} \\ \tau_{xy} \end{Bmatrix} = \frac{K_{\mathrm{I}}}{\sqrt{2\pi r}} \cos\frac{\theta}{2} \begin{Bmatrix} 1-\sin\frac{\theta}{2}\sin\frac{3\theta}{2} \\ 1+\sin\frac{\theta}{2}\sin\frac{3\theta}{2} \\ \sin\frac{\theta}{2}\cos\frac{3\theta}{2} \end{Bmatrix}. \qquad (1)$$

For mode I cracks, the boundary condition $\tau_{xy} = 0$ along the *x* axis is automatically satisfied from the above equation. Westergaard equations, which were originally developed for a biaxial stress field, were subsequently applied for uniaxial loading. However, they produce a σ_{xx} component at the boundary edges along the crack axis for a purely uniaxial load. To satisfy the boundary condition also under uniaxial loading, Irwin [25] suggested the use of a transverse component of stress, namely the *T*-stress. This was consolidated later by Williams [7]. He showed that the crack-tip stress fields in an isotropic elastic material can be expressed as an infinite power series, where the leading term exhibits a singularity $r^{-1/2}$, the second term is constant with *r*, the third term is proportional to $r^{1/2}$, and so on. Although the third and higher terms in the Williams solution vanish at the crack tip, the second (uniform) term remains finite. This second term can have a profound effect on the plastic zone shape and the stresses deep inside the plastic zone [26].

In general, near the crack tip of an isotropic elastic material, where only the first two terms of Williams solution are considered, stresses can be written as follow:

for mode I

$$\sigma_{xx} = \frac{K_{\mathrm{I}}}{\sqrt{2\pi r}}\cos\frac{\theta}{2}\left[1-\sin\frac{\theta}{2}\sin\frac{3\theta}{2}\right] + T + O(r^{1/2}),$$

$$\sigma_{yy} = \frac{K_{\mathrm{I}}}{\sqrt{2\pi r}}\cos\frac{\theta}{2}\left[1+\sin\frac{\theta}{2}\sin\frac{3\theta}{2}\right] + O(r^{1/2}), \qquad (2)$$

$$\tau_{xy} = \frac{K_{\mathrm{I}}}{\sqrt{2\pi r}}\cos\frac{\theta}{2}\sin\frac{\theta}{2}\sin\frac{3\theta}{2} + O(r^{1/2}).$$

for mode II

$$\sigma_{xx} = \frac{K_{\mathrm{II}}}{\sqrt{2\pi r}}\sin\frac{\theta}{2}\left[2+\cos\frac{\theta}{2}\cos\frac{3\theta}{2}\right] + O(r^{1/2}),$$

$$\sigma_{yy} = \frac{K_{\mathrm{II}}}{\sqrt{2\pi r}}\sin\frac{\theta}{2}\cos\frac{\theta}{2}\cos\frac{3\theta}{2} + O(r^{1/2}), \qquad (3)$$

$$\tau_{xy} = \frac{K_{\mathrm{II}}}{\sqrt{2\pi r}}\cos\frac{\theta}{2}\left[1-\sin\frac{\theta}{2}\sin\frac{3\theta}{2}\right] + O(r^{1/2}),$$

where K_{I} and K_{II} are the mode I and mode II stress intensity factors, and *r*, θ, *x* and *y* are coordinates in conventional polar and Cartesian systems (with the crack tip assumed as the origin). The term *T* represents a uniform stress in the *x* direction, parallel to the crack tip. It is only due to a symmetric component of loading and vanishes for pure mode II. When $T = 0$, small-scale yielding can be assumed and the plastic zone is a negligible fraction of the crack length as well as of the entire body. The stress intensity factors are,

in these conditions, able to uniquely characterize the near-tip fields.

To normalize the effect of T relative to the stress intensity factor in mode I, a dimensionless parameter called the biaxiality ratio B is used, as introduced and defined by [13]

$$B = \frac{T\sqrt{\pi a}}{K_{\mathrm{I}}}, \tag{4}$$

where a is the crack length. For a through-thickness crack in an infinite plate subject to a remote normal stress, $B = -1$. Thus a remote stress σ induces a T-stress of $-\sigma$ in the x direction.

The biaxiality parameter B can be extended to mixed mode if K_{I} is replaced by an effective stress intensity factor

$$K_{\mathrm{eff}} = \sqrt{K_{\mathrm{I}}^2 + K_{\mathrm{II}}^2}. \tag{5}$$

Several numerical methods have been developed for estimating the T-stress, such as the weight function technique and the stress difference method. The weight function or Green function approach [27] was based on an analytical representation of the elastic stress on isotropic material. This method for evaluating T-stress results easy to implement with quite accurate results. The stress difference method [28] evaluates the T-stress by subtracting the stresses σ_{xx} and σ_{yy} calculated close to the crack tip. The method is easy to define and to apply, with a good accuracy.

However the applicability of the above mentioned techniques, not implemented in finite element codes, is limited to simple geometry and loading configurations. Ayatollahi et al. [23] provided a technique for evaluating T-stress for mode I and II, involving a unified finite element analysis.

3. FINITE ELEMENT METHOD FOR THE EVALUATION OF T-STRESS: MODE I AND MIXED MODE FORMULATION

Considering mode I loading, Eqs. (2) show that σ_{xx} comprises of the singular term and T, while higher order terms are negligible. This implies that T can be determined along any direction where the singular term of σ_{xx} vanishes or can be set to zero by superposing with a fraction of σ_{yy}. This corresponds to different angular positions around the crack tip, such as when

$$\theta = -\pi \text{ or } +\pi\text{: } T = \sigma_{xx}. \tag{6}$$

This approach is very easy and straightforward since it uses only one stress component. By the way, if analytical results are compared with finite element analyses, a very refined and accurate mesh is required to obtain good agreement. Alternative solution to this problem is to compute the T-stress using the displacements along the crack faces. Due to traction free boundary conditions along the crack faces, Hooke's law can be written for small strains as

$$\sigma_{xx} = E'\varepsilon_{xx} = \frac{E'\mathrm{d}u_x}{\mathrm{d}x}, \tag{7}$$

where ε_{xx} and u_x are the strain and displacement respectively parallel to the crack and

$$E' = \begin{cases} E, & \text{plane stress,} \\ \dfrac{E}{1-\nu^2}, & \text{plane strain.} \end{cases} \tag{8}$$

For the chosen angular position around the crack tip of Eq. (6), the singular term of σ_{xx} in Eq. (2) disappears and Hooke's law becomes

$$T = \frac{E'\mathrm{d}u_x}{\mathrm{d}x}. \tag{9}$$

Recalling that T is constant and replacing the constant slope $\mathrm{d}u_x/\mathrm{d}x$ with $(u_x(x) - u_x(0))/x$, T can be defined as [23]

$$T = E'(u_x(x) - u_x(0))/x, \tag{10}$$

where $u_x(0)$ denotes u_x at the crack tip.

This indicates that using either u_x or its slope along the crack faces T can be determined directly from finite element results. This approach permits to obtain the T-stress for mode I loading with the employment of a coarse mesh since, as well known, the displacements are in general not affected by the mesh refinement.

Different considerations must be done when mixed mode loading is considered. In fact, along any radial direction from the crack tip, there is a singular term due to either mode I or mode II or both. For this reason, the singular term σ_{xx} never vanishes, and the method described for mode I is not therefore suitable for mixed mode I/II loading. However, the T-stress can be found when the symmetric properties of mode I and antisymmetric properties of mode II for direct stresses are used, without the calculation of stress intensity factors. The stresses in one half of the cracked specimen are added to those of the other half. The mode II stresses vanish and mode I stresses are doubled. As a consequence, again like under mode I loading, the T-stress can be determined along any direction around the crack tip directly from finite element results. The most convenient direction is $\theta = \pm\pi$ since only one component of stress is involved

$$T = 1/2[(\sigma_{xx})_{\theta=-\pi} + (\sigma_{xx})_{\theta=\pi}]. \tag{11}$$

Following now similar steps presented for mode I loading, T under mixed mode loading can be determined employing the displacement method, leading to

$$T = \frac{1}{2x} E' \left[u_x(x, -\pi) + u_x(x, \pi) \right]. \quad (12)$$

Since the path independent integral J for mixed mode loading is usually available from the finite element analysis, the biaxiality ratio B for mixed mode conditions is

$$B = T \sqrt{\frac{\pi a}{JE'}}, \quad (13)$$

where $K_{\text{eff}} = \sqrt{JE'}$.

Equation (13) together with Eq. (12) or (11) can be used to determine B without having to calculate separately K_{I} and K_{II} and directly from finite element analysis.

The method developed by [23] was verified to several test cases by using ABAQUS. Finite element results for T were obtained for two different mode I cracked specimens: a single edge notched (SEN) and a double edge notched (DEN). For the SEN specimen the crack length a to width W ratio was 0.4 and for the DEN specimen a/W was 0.2. Both the stress and the displacement methods were used to determine T for distances x behind the crack tip and along the crack face. For identical meshes the stress method did not provide a constant value for T/σ_{nom}, where σ_{nom} is the uniform far field tensile stress. For mixed mode conditions, T was calculated for an inclined edge crack in a large square plate, by applying stress and displacement methods as well. It was found that both the stress and displacement methods gave results that compare well with the analytical results from [22].

The outcomes of [23] are based on applications carried out for the same accurate mesh refinement. A study on the effects of the mesh refinement is provided in the present paper, concerning the accuracy of the displacement methods. The results obtained for mode I loading and mode I/II loading are presented considering SEN, DEN specimens and centrally cracked plate.

4. EVALUATION OF *T*-STRESS WITH COARSE ESHES UNDER MODE I LOADING

4.1. Geometry and Loads

In order to investigate the effect of the mesh refinement on the T-stress evaluation and to study the sensitivity to this aspect of the displacement method as introduced in [23], several finite element analyses have been carried out. The single edge notched and double edge notched specimens which are investigated for the T-stress evaluation under mode I are shown in Fig. 1. Three different mesh types are modeled. The first applied mesh is a fine and detailed mesh. The second mesh is a coarse mesh, intended to be less complex and heavy than the previous one. The third modeled mesh is a very coarse mesh: this is done to observe how the accuracy of the results modifies by reducing the mesh refinement.

The SEN specimen is defined to match the same non-dimensional properties of the samples used in [23], where the ratio a/W is 0.4. It is realized by assuming the crack length $a = 20$ mm and the width $W = 100$ mm. The height of the specimen $2H$ is equal to 200 mm so that the uniform far field tensile stress σ_{nom} is applied far enough from the crack. Due to symmetry, only one half of the SEN is considered.

The DEN specimen [23] presents a ratio a/W of 0.2, and it is obtained by keeping $W = 100$ mm and by reducing the crack length to $a = 20$ mm. In this case $2H = 200$ mm. Due to symmetry, only one quarter of the DEN specimens is modeled. Uniform far field tensile stress σ_{nom} equal to 100 MPa is applied. The geometries and loading conditions are modeled and analyzed by means of the finite element code ANSYS and Solid 8 node 183 element is used. The analyses have been carried out under linear elastic and plane strain conditions. Young's modulus $E = 206$ GPa and $\nu = 0.3$ are assumed.

4.2. Fine Mesh

Very fine mesh is first analyzed for the SEN and DEN specimens. The mesh is realized by regularly distributed elements. The number of elements becomes very high around the crack tip: the smallest element size approached the order of 10^{-6}, and the number of

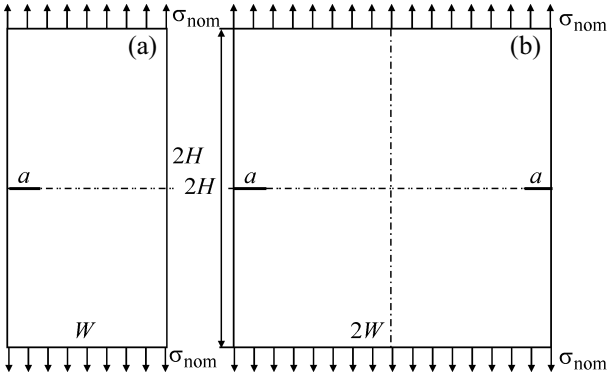

Fig. 1. Single (a) and double edge notched specimens (b).

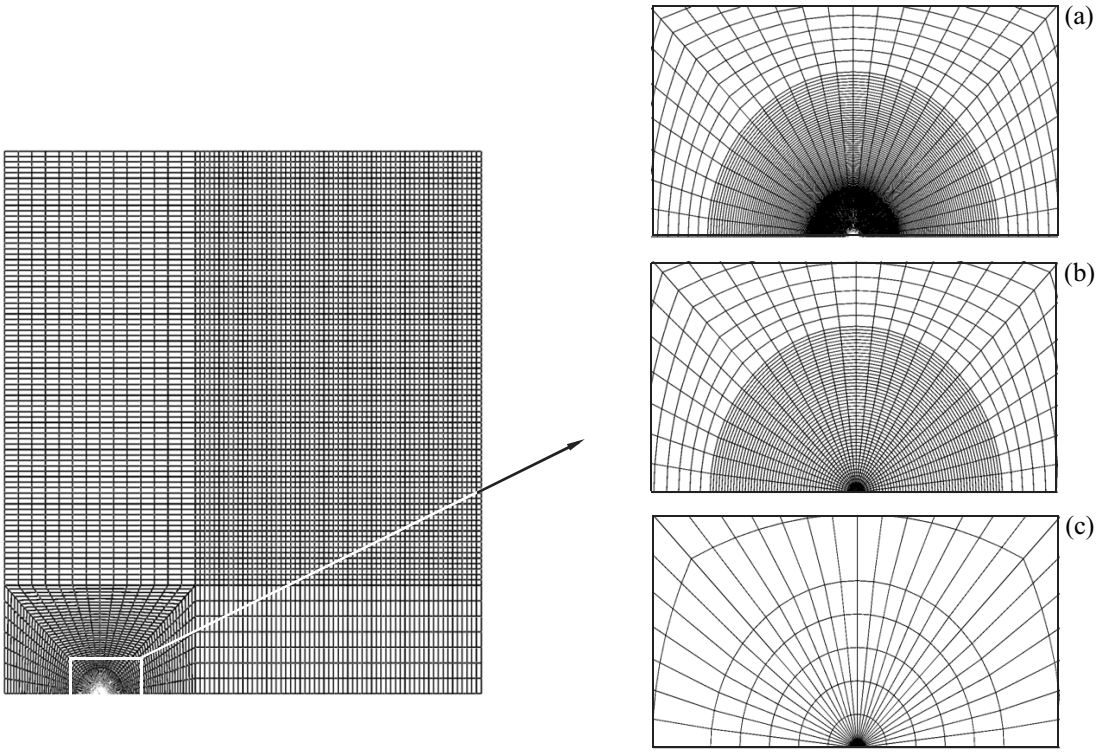

Fig. 2. An example of fine mesh for the DEN specimen and variants for the crack tip: fine (a), coarse (b) and very coarse mesh (c).

elements used for meshing the DEN model was about 18 000. Example is given in Fig. 2 only for the DEN specimen, for the sake of brevity.

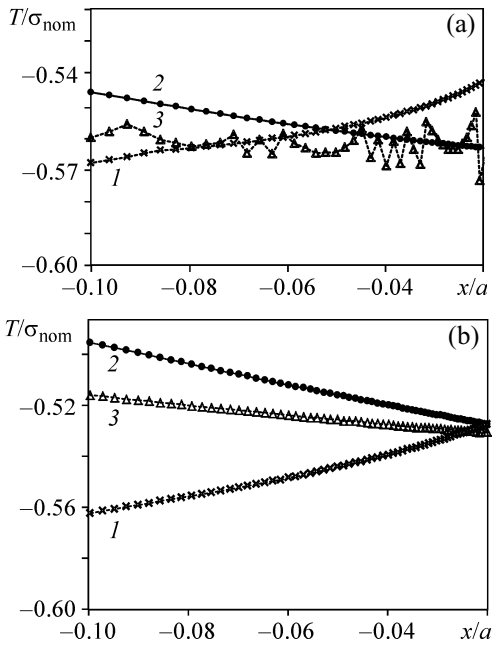

Fig. 3. *T*-stress results for SEN (a) and DEN specimens (b) by using a fine mesh: stress method for $\theta = 0$ (*1*) and π (*2*); displacement method for $\theta = \pi$ (*3*).

A fine mesh gives more accurate results. The difficulties become more evident when complex geometries are involved.

Firstly, the stress method is applied along the direction $\theta = 0$. According to this method, the *T*-stress is evaluated as

$$T = \sigma_{xx} - \sigma_{yy}.$$

The stress method is also applied assuming $\theta = \pi$ for the upper face of the specimen and *T*-stress is then evaluated according to Eq. (6).

The final case is the application of the displacement method for $\theta = \pi$: *T*-stress is evaluated according to Eq. (10).

A comparison of the results for the fine mesh case, by applying the three different techniques, is presented in Fig. 3a for the SEN specimen and in Fig. 3b for the DEN specimen for mode I. The obtained *T*-stress divided by the nominal stress σ_{nom} is plotted as function of the distance from the crack tip divided by the crack length x/a.

For the SEN specimen (Fig. 3a) it is observed for all the three applied techniques a poor dispersion of the results that are within the range from –0.54 to –0.57 for the analyzed range of distances from the crack tip. It is possible to observe the same behavior also for the DEN specimen results (Fig. 3b) that remain within

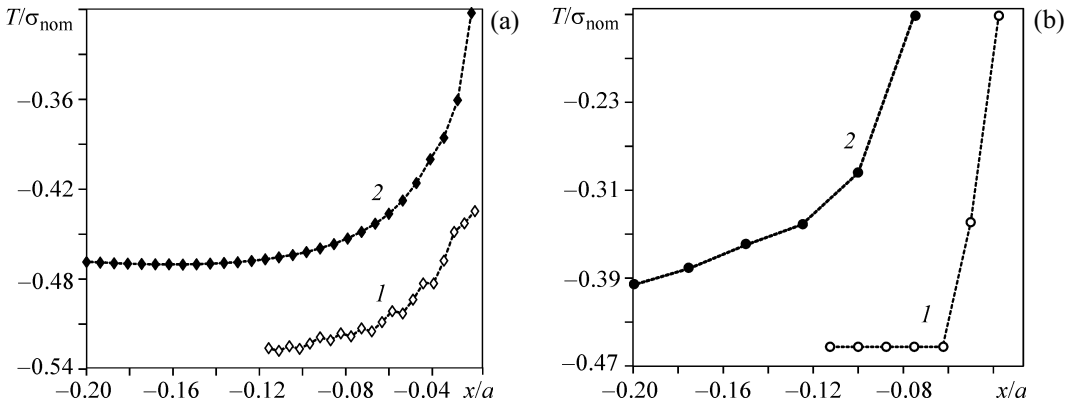

Fig. 4. *T*-stress for the SEN (*1*) and DEN specimens (*2*) modeled by a coarse (a) and very coarse mesh (b); displacement method for $\theta = \pi$.

the range from –0.50 to –0.56 for the analyzed range of distances from the crack tip. In [23] T/σ_{nom} calculated from the displacement method for the SEN and DEN specimens were equal to –0.55 and –0.506 respectively, for fine mesh.

These outcomes for the SEN and DEN specimen confirm that the displacement method gives reliable and accurate results, compared to the stress method, although this one is more known and applied.

It is also possible to observe that for the SEN specimen the curve obtained by the displacement method, except for some fluctuations of the results, shows a constant behavior (Fig. 3a).

The displacement method results for the DEN specimen show an almost constant behavior with a variation of T/σ_{nom} of less than 0.01.

The stress method for $\theta = 0$ shows an increasing trend, while for $\theta = \pi$ it has a decreasing trend for both the SEN and DEN specimens (Fig. 3) with larger variation of the T/σ_{nom} results.

4.3. Coarse Mesh

The second mesh type, realized for the SEN and DEN specimens, is a coarse mesh. This coarse mesh refinement is assumed aiming to check if a reliable estimation of the *T*-stress is possible without a detailed fine mesh. Clearly, a fine mesh is more complex and requires more computational power and time, thus reducing the number of analysis in the same time frame.

The coarse mesh has a reduced number of elements that are less dense around the crack tip than the fine mesh modeling, and the smallest element size is reduced to the order of 10^{-1}. The number of elements used for meshing the DEN model was about 4000. Also in this case the mesh elements are regularly distributed, increasing around the crack tip.

The displacement method is based on nodal displacements that are not influenced by the mesh definition, making this technique suited for any type of mesh. The same is not true for the stress evaluation. Thus, for coarse meshes, the stress method is disregarded.

In Fig. 4a the *T*-stress calculated for the displacement method on the coarse mesh is presented for the SEN and DEN specimens. The obtained results for the SEN specimen show that the *T*-stress varies significantly getting closer to the crack tip. In particular the ratio T/σ_{nom} shifts rapidly to an almost constant *T*-stress value of –0.50 to –0.52 for x/a greater than –0.06. For the DEN specimen the coarse mesh results start diverging from a constant value of T/σ_{nom} for x/a greater than –0.08, up to a value of T/σ_{nom} of –0.3.

4.4. Very Coarse Mesh

The last modeled mesh is a very coarse mesh. The main aim is to check the accuracy of the results keeping reducing the mesh refinement. The very coarse mesh is characterized by a sparse distribution of the mesh elements. Mesh elements are regularly distributed, increasing around the crack. The smallest element size at the crack tip is 1 mm. Only 800 elements were used to mesh the DEN model. In this case only the displacement method is applied, assuming $\theta = \pi$.

The *T*-stress calculated for the SEN and the DEN specimens on the very coarse mesh is presented in Fig. 4b. The *T*-stress varies significantly getting closer to the crack tip; this behavior, already observed for the coarse mesh (see Fig. 4a), becomes now more evident. For the SEN specimen, T/σ_{nom} remains constant and

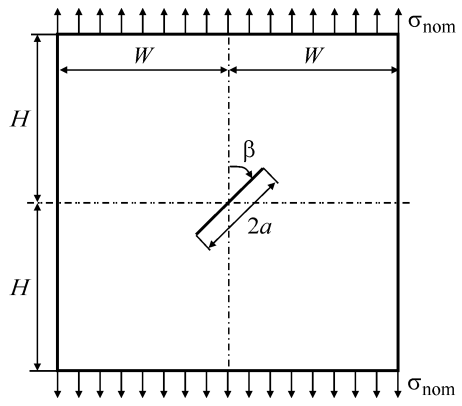

Fig. 5. Large square plate for mixed mode I/II loading condition.

almost equal to –0.45 for x/a less than –0.06 and then it diverges. The *T*-stress calculated for the DEN specimen on the very coarse mesh does not show a constant behavior in the observed ranges of x/a.

5. EVALUATION OF *T*-STRESS WITH COARSE MESHES UNDER MIXED MODE I/II LOADING

5.1. Geometry and Loads

In this section the applications for the mixed mode I/II are reported. Plate with a central crack is considered. The three different mesh refinements are modeled and analyzed. The analysis of the influence of the mesh refinements on the accuracy of the *T*-stress is conducted only for displacement method. In order to keep a similarity with the analysis of [23], the only known dimension is the angle between σ_{nom} and the crack direction, denoted by β (when β = 0 mode II condition applies, and when β = 90° mode I condition applies). In the following calculations the angle β is set equal to 70°. The large square plate for the mixed mode I/II is modeled assuming two different crack length defined as $2a$ = 2 and 40 mm (Fig. 5). The width is chosen equal to $2W$ = 200 mm and the height $2H$ = 200 mm.

The *T*-stress evaluation to mode I/II for the two different crack lengths of the square plate is carried out by applying a uniform far field tensile stress σ_{nom} equal to 100 MPa.

The geometries and loading conditions are modeled and analyzed by means of the finite element code ANSYS and Solid 8 node 183 element is used. The considered material is linear elastic isotropic having E = 206 GPa, and ν = 0.3. Plane strain condition is assumed.

Since it is not possible to apply symmetry constrains to the cracked square plate, the geometry is fully modeled.

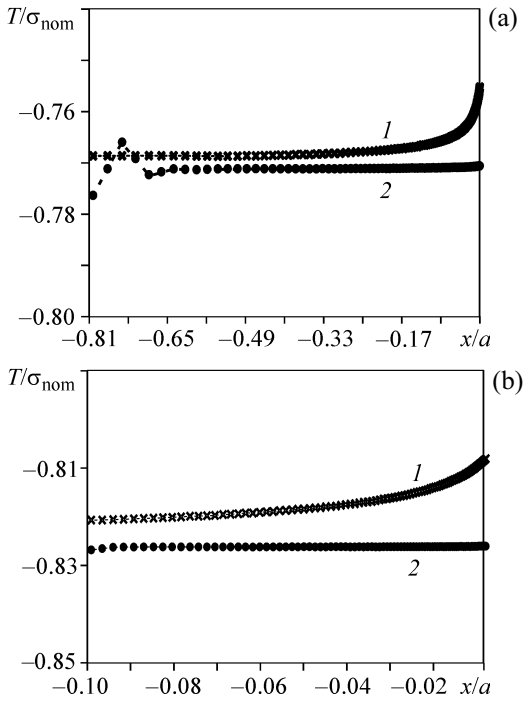

Fig. 6. Square plate with the crack length $2a$ = 2 (a) and 40 mm (b); stress method with θ = 0 (*1*) and ±π (*2*), fine mesh.

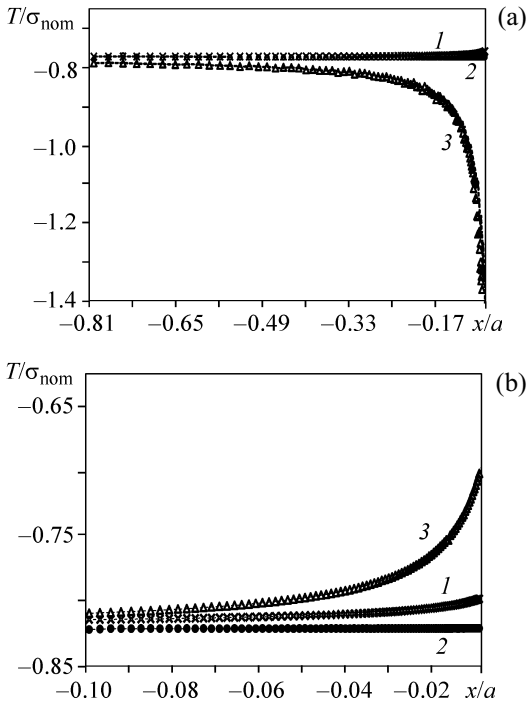

Fig. 7. Square plate with the crack length $2a$ = 2 (a) and 40 mm (b); stress method with θ = 0 (*1*) and ±π (*2*), and displacement method with θ = ±π (*3*), fine mesh.

5.2. Fine Mesh

The mesh is realized by finite regularly distributed elements becoming denser around the crack tip. The size of elements and other conditions to define the mesh as "fine" are the same reported in the Sect. 4.2. For the fine mesh case, three different techniques for evaluating *T*-stress are applied.

The first one is the stress method assuming $\theta = 0$. According to this method the *T*-stress is evaluated as:

$$T = (\sigma_{xx} - \sigma_{yy})_{\theta=0}.$$

The second application is carried out by applying the stress method assuming $\theta = \pi$ at the upper face of the plate and $\theta = -\pi$ at the lower face. This is done in accordance with Eq. (11).

A comparison of the *T*-stress results by applying the stress method assuming $\theta = 0$ and $\theta = \pm\pi$ is presented in Fig. 6 for the square plate with a crack length $2a = 2$ mm. The stress method with $\theta = 0$ and $\theta = \pm\pi$ gives almost the same results for the investigated range of distance from the crack tip.

The third technique applied to the fine mesh is the displacement method assuming $\theta = \pi$ at the upper face of the plate and $\theta = -\pi$ at the lower face. This is done in accordance with Eq. (12).

In Fig. 7 the comparisons of the results for the three different techniques, respectively for the square plate with $2a = 2$ mm and 40 mm are shown. *T*-stress results for the displacement method remain generally close to the stress method results and diverges only in the vicinity of the crack tip. In particular from Fig. 7a for $2a = 2$ mm, the three applied techniques provide the same value of the *T*-stress in the range x/a between -0.81 and -0.1 and only after $x/a = -0.1$ the displacement method starts diverging. Also for the square plate with $2a = 40$ mm (Fig. 7b) the three techniques show almost the same *T*-stress results in the range x/a between -0.1 and -0.05 with a limited variation of T/σ_{nom}.

Is it possible to conclude that the displacement method gives reliable results also for the square plate under mixed mode I/II. The method provides a good assessment of the *T*-stress also in case of a large crack length, comparable to the plate width.

5.3. Coarse Mesh

The second mesh type, realized for the square plate with $2a = 2$ mm and 40 mm, is the coarse mesh.

The coarse mesh has regularly distributed elements, increasing around the crack tip but with a reduced number of elements compared to the fine mesh modeling (see Sect. 4.3 for the element size).

The stress method for coarser mesh is disregarded and only the displacement method is considered.

The displacement method assuming $\theta = \pi$ at the upper face of the plate and $\theta = -\pi$ at the lower face is applied. The *T*-stress results obtained for the square plate with the crack lengths $2a = 2$ mm and 40 mm modeled by a coarse mesh are shown respectively in Fig. 8. In both cases the *T*-stress results remain almost constant and diverge only in the vicinity of the crack tip.

5.4. Very Coarse Mesh

The very coarse mesh is characterized by a sparse distribution of the mesh elements (regularly distributed, increasing around the crack tip as described in Sect. 4.4). The main aim is to check the accuracy of the results by applying the displacement method with $\theta = \pm\pi$ keeping reducing the mesh refinement. The *T*-stress results obtained for the square plate with the crack lengths $2a = 2$ mm and 40 mm modeled by very coarse mesh are shown in Fig. 9. The *T*-stress results, for both the crack lengths, remain almost constant and diverge only in the vicinity of the crack tip. The displacement method applied to the very coarse mesh seems to provide a reliable *T*-stress estimation even with a very light and easy mesh type.

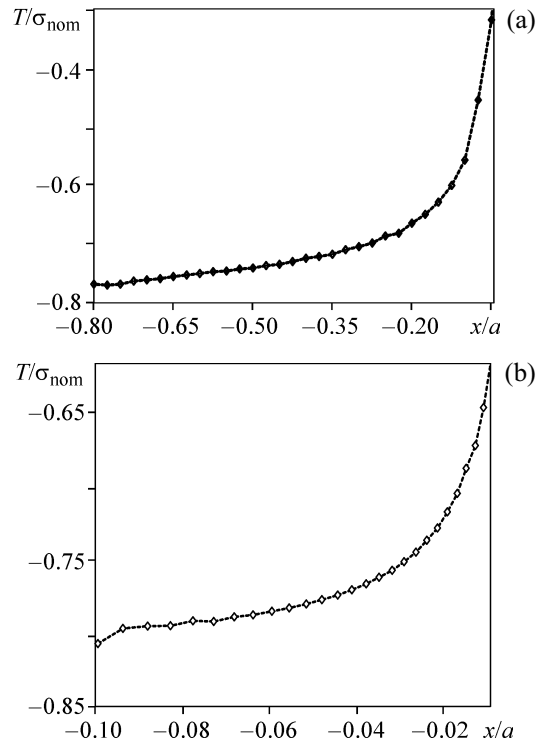

Fig. 8. Square plate with the crack length $2a = 2$ (a) and 40 mm (b); displacement method with $\theta = \pm\pi$, coarse mesh.

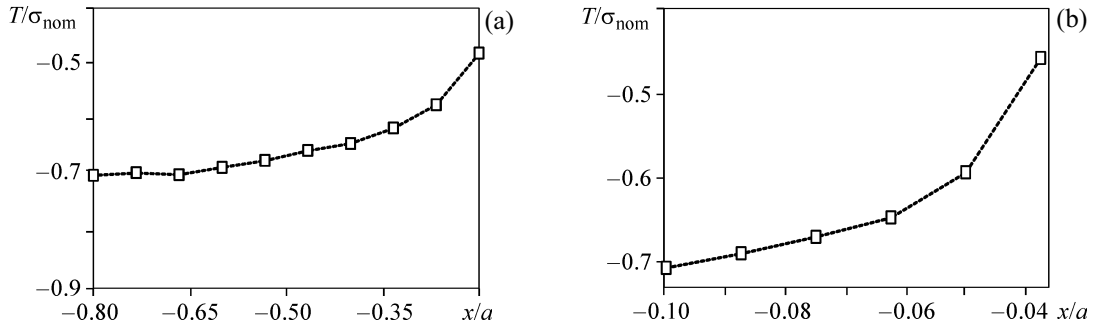

Fig. 9. Square plate with the crack length $2a = 2$ (a) and 40 mm (b); displacement method with $\theta = \pm\pi$, very coarse mesh.

6. SYNTHESIS OF THE RESULTS AND DISCUSSION

6.1. Mode I Loading

A comparison between the three mesh refinement results is reported, for the mode I loading in Fig. 10a for the SEN specimen and in Fig. 10b for the DEN specimen.

For both cases, it is possible to observe that the outcomes of the fine mesh, by the application of different methods, remain uniform and characterized by an almost constant value of the *T*-stress, in the investigated range of distance from the crack tip. It has been already discussed that the displacement and the stress method, applied to the fine mesh, show a fine agreement with the results [23]. For the SEN specimen (Fig. 10a) coarse and fine mesh results differ of 0.03. The discrepancy of the two methods remains limited to this value in a range of x/a between –0.1 and –0.06. It becomes more evident in the vicinity of the crack tip. It is also evident that the coarser is the mesh element size, the smaller are the *T*-stress results. In particular, the very coarse mesh curve differs of 0.06 from the coarse mesh and 0.11 from the fine mesh, in the same range x/a.

A more evident discrepancy in the outcomes of the coarser mesh is also observed comparing the DEN specimen results (Fig. 10b). The coarse mesh provides *T*-stress values that in the range x/a between –0.18 and –0.08 differ from the fine mesh of 0.05. Also in this case the calculated values of the *T*-stress reduce by decreasing the mesh refinement with a difference of 0.17 with the fine mesh results and 0.12 with the coarse mesh.

All these considerations for the mode I loading, for the SEN and DEN specimens, denote that there is a limit in reducing the mesh refinement: under this limit, the *T*-stress results could become inaccurate.

6.2. Mixed Mode I/II Loading

A comparison between the different mesh refinement results is reported in Fig. 11 for a crack length of $2a = 2$ mm and 40 mm. For both the analyzed geom-

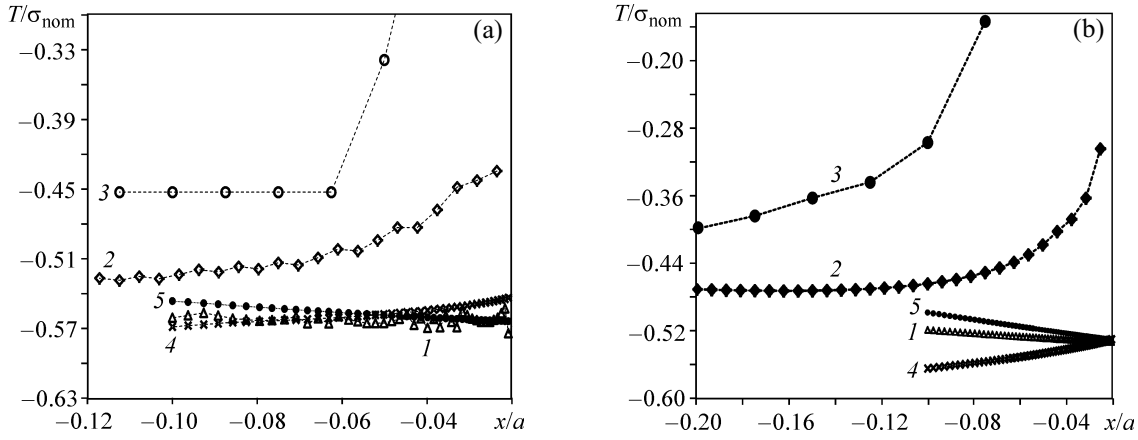

Fig. 10. Comparison of the results for the SEN (a) and DEN (b) specimens: displacement method with fine (*1*), coarse (*2*) and very coarse mesh (*3*) refinements; stress method with fine mesh: $\theta = 0$ (*4*) and π (*1–3*, *5*).

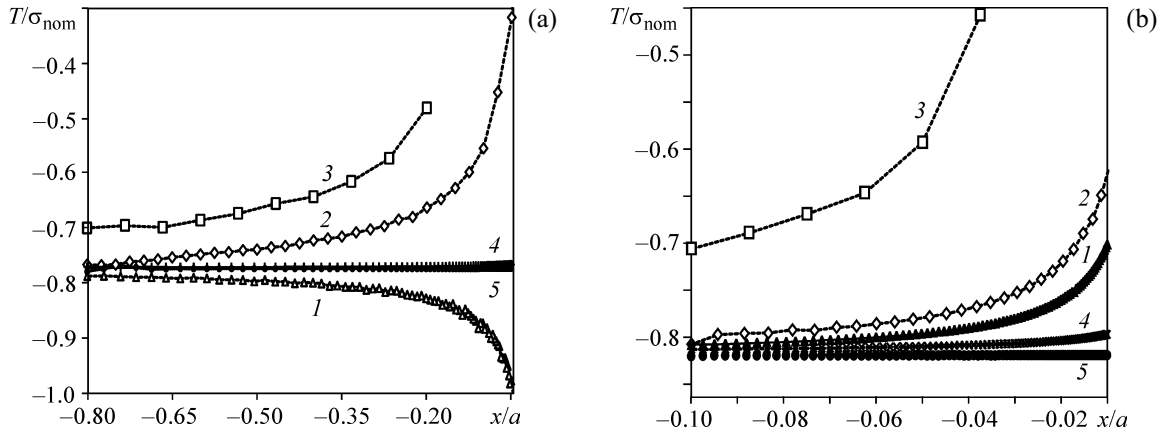

Fig. 11. Comparison of the results for the square plate with $2a = 2$ (a) and 40 mm (b): displacement method with fine (*1*), coarse (*2*) and very coarse (*3*) mesh refinements; stress method with fine mesh: $\theta = 0$ (*4*) and $\pm\pi$ (*1–3*, *5*).

etries, the fine mesh applications by stress and displacement methods provide good and reliable results of the *T*-stress. From the comparison between the different mesh refinements it is possible to observe that for mixed mode I/II the displacement method, applied to the coarse and to the very coarse meshes, still provides reliable results. For the crack length $2a = 2$ mm (Fig. 11a), the coarse mesh results and the very coarse mesh results differ of less than 0.1 from the fine mesh results in the range of x/a between –0.81 and –0.31. All the results, far from the crack tip, converge to the same value of the *T*-stress.

For the crack length $2a = 40$ mm (Fig. 11b) the comparison of results shows a good agreement of the *T*-stress evaluation by using coarse and very coarse mesh. In particular in the range of x/a between –0.09 and –0.03, there are differences of less than 0.05 with the *T*-stress obtained by using the fine mesh. The convergence of the results in the same *T*-stress value far from the crack tip is observed also for this case.

In Fig. 11, the results for the very coarse and regular mesh are introduced and compared with the others. It is quite evident how the differences in *T*-stress values increase although the behavior is similar to the coarse and very coarse mesh curves. The regular type of elements used for the same refinement modifies the *T*-stress outcomes. These results are still characterized by small differences with the others far from the crack tip.

Generally it is possible to conclude that for the mixed mode I/II the mesh refinement does not affect the accuracy of the *T*-stress far from the crack tip but in case of the very coarse mesh, the type of mesh elements used for the same mesh refinement can influence the accuracy of the *T*-stress results.

7. CONCLUSION

In this paper the method presented in [23] for evaluating the *T*-stress is applied by assuming different mesh refinements. The final aim is to investigate the reliability of that approach depending on different mesh refinements for mode I and for mixed mode loading. It emerges that, despite the stress method is more known and applied, also the displacement method gives good and reliable results for evaluating the *T*-stress.

All the models showed that discrepancy between *T*-stress values becomes more evident close to the crack tip. This is mainly due to the localized high stresses.

Under mode I loading, reasonable errors are obtained for a coarse mesh and the *T*-stress can be evaluated using coarse mesh.

For very coarse mesh and mode I loading, discrepancy on the *T*-stress evaluation becomes evident. There is a lower limit on the mesh refinement over which the *T*-stress values are not reliable.

For the mixed mode I/II the mesh refinement does not reduce the accuracy of the *T*-stress result far from the crack tip and the method provides a good assessment of the *T*-stress also in case of a large crack length, comparable to the plate width.

When fine meshes are employed, the *T*-stress presents a very reduced scatter and good results are obtained for all the geometries. The results from displacement and stress method are comparable diverging only in the proximity of the crack tip.

In conclusion, the displacement method permits the evaluation of the *T*-stress with the employment of coarse meshes. By the way, several precautions must be taken when dealing with coarse and very coarse meshes.

REFERENCES

1. McClintock, F.A., *Plasticity Aspect of Fracture, Fracture an Advanced Treatise*, Vol. III, Liebowitz, H., Ed., New York: Academic Press, 1971, pp. 47–225.
2. O'Dowd, N.P. and Shih, C.F., Family of Crack-Tip Fields Characterized by a Triaxiality Parameter—I. Structure of fields, *J. Mech. Phys. Solid.*, 1991, vol. 39, pp. 989–1015. doi 10.1016/0022-5096(91)90049-T
3. O'Dowd, N.P. and Shih, C.F., Family of Crack-Tip Fields Characterized by a Triaxiality Parameter—II. Fracture Applications, *J. Mech. Phys. Solid.*, 1992, vol. 40, pp. 939–963. doi 10.1016/0022-5096(92)90057-9
4. Shih, C., O'Dowd, N., and Kirk, M., *A Framework for Quantifying Crack Tip Constraint, Constraint Effects in Fracture*, West Conshohocken, PA: ASTM Int., 1992, pp. 2–19. doi 10.1520/STP18020S
5. Ayatollahi, M.R., Rashidi Moghaddam, M., Razavi, N., and Berto, F., Geometry Effects on Fracture Trajectory of PMMA Samples under Pure Mode-I Loading, *Eng. Fract. Mech.*, 2016, vol. 163, pp. 449–461. doi 10.1016/j.engfracmech.2016.05.014
6. Rashidi Moghaddam, M., Ayatollahi, M.R., Razavi, N., and Berto, F., Mode II Brittle Fracture Assessment Using an Energy Based Criterion, *Phys. Mesomech.*, 2017, vol. 20, no. 2, pp. 142–148.
7. Williams, M.L., On the Stress Distribution at the Base of a Stationary Crack, *J. Appl. Mech.*, 1957, vol. 24, pp. 109–114. doi 10.1115/1.3640470
8. Hancock, J., Reuter, W., and Parks, D., *Constraint and Toughness Parameterized by T*, West Conshohocken, PA: ASTM Int., 1993. doi 10.1520/STP18021S
9. Sumpter, J.D.G., *An Experimental Investigation of the T Stress Approach*, ASTM STP 1171, 1993, pp. 492–502. doi 10.1520/STP18042S
10. Sherry, A.H., France, C.C., and Goldthorpe, M.R., Compendium of T-Stress Solutions for Two and Three Dimensional Cracked Geometries, *Fatig. Fract. Eng. Mater. Struct.*, 1995, vol. 18, pp. 141–155. doi 10.1111/j.1460-2695.1995.tb00148.x
11. Chen, Y.Z., Integral Equation Methods for Multiple Crack Problems and Related Topics, *Appl. Mech. Rev.*, 2007, vol. 60, no. 172. doi 10.1115/1.2750671
12. Larsson, S.G. and Carlsson, A.J., Influence of Non-Singular Stress Terms and Specimen Geometry on Small-Scale Yielding at Crack Tips in Elastic-Plastic Materials, *J. Mech. Phys. Solid.*, 1973, vol. 21, pp. 263–277. doi 10.1016/0022-5096(73)90024-0
13. Leevers, P.S. and Radon, J.C., Inherent Stress Biaxiality in Various Fracture Specimen Geometries, *Int. J. Fract.*, 1982, vol. 19, pp. 311–325. doi 10.1007BF00012486
14. Ewing, P.D., Swedlow, J.L., and Williams, J.G., Further Results on the Angled Crack Problem, *Int. J. Fract.*, 1976, vol. 12, pp. 85–93. doi 10.1007/BF00036011
15. Knesl, Z., Evaluation of the Elastic T-Stress Using a Hybrid Finite Element Approach, *Int. J. Fract.*, 1994, vol. 70, pp. R9–R14. doi 10.1007/BF00018140
16. Cardew, G.E., Goldthorpe, M.R., Howard, I.C., and Kfouri, A.P., On the Elastic T-Term, in *Fundamental Deformation and Fracture*, Bilby, B.A., Miller, K.J., and Willis, J.R., Eds., Sheffield: Cambridge University Press, 1984, pp. 465–476.
17. Kfouri, A.P., Some Evaluations of the Elastic T-Term Using Eshelby's Method, *Int. J. Fract.*, 1986, vol. 30, no. 301–315. doi 10.1007/BF00019710
18. Fett, T., A Green's Function for T-Stresses in an Edge-Cracked Rectangular Plate, *Eng. Fract. Mech.*, 1997, vol. 57, pp. 365–373. doi 10.1016/S0013-7944(97)00034-9
19. Maleski, M.J., Kirugulige, M.S., and Tippur, H.V., A Method for Measuring Mode I Crack Tip Constraint under Static and Dynamic Loading Conditions, *Exp. Mech.*, 2004, vol. 44, pp. 522–532. doi 10.1007/BF02427964
20. Olsen, P.C., Determining the Stress Intensity Factors K_I, K_{II} and the T-Term Via the Conservation Laws Using the Boundary Element Method, *Eng. Fract. Mech.*, 1994, vol. 49, pp. 49–60. doi 10.1016/0013-7944(94)90110-4
21. Sladek, J., Sladek, V., and Fedelinski, P., Contour Integrals for Mixed-Mode Crack Analysis: Effect of Nonsingular Terms, *Theor. Appl. Fract. Mech.*, 1997, vol. 27, pp. 115–127. doi 10.1016/S0167-8442(97)00013-X
22. Seed, G.M. and Nowell, D., Use of the Distributed Dislocations Method to Determine the T-Stress, *Fatigue Fract. Eng. Mater. Struct.*, 1994, vol. 17, pp. 605–618.
23. Ayatollahi, M.R., Pavier, M.J., and Smith, D.J., Determination of T-Stress from Finite Element Analysis for Mode I and Mixed Mode I/II Loading, *Int. J. Fract.*, 1998, vol. 91, pp. 283–298. doi 10.1023/A:1007581125618
24. Westergaard, H.M., Bearing Pressures and Cracks, *J. Appl. Mech.*, 1939, vol. 61, pp. A49–A53. doi 216756690
25. Irwin, G.R., Fracture, in *Elasticity and Plasticity*, Flügge, S., Ed., Berlin–Heidelberg: Springer, 1958, pp. 551–590. doi 10.1007/978-3-642-45887-3_5
26. Anderson, T.L., *Fracture Mechanics: Fundamentals and Applications*, Taylor & Francis, 2005.
27. Bueckner, H., *A Novel Principle for the Computation of Stress Intensity Factors*, 1970.
28. Yang, Y.Y., Effect of the Regular Term on the Stress Field in a Joint of Dissimilar Materials under Remote Mechanical Load, *Arch. Appl. Mech.*, 1999, vol. 69, pp. 364–378. doi 10.1007/s004190050227